MODELING OF A FIBER-OPTIC HUMIDITY SENSOR BASED ON A CARRAGEENAN-COATED FABRY-PEROT INTERFEROMETER

M. M. Khasanov
Independent researcher, Tashkent State Technical University named after Islam Karimov
https://doi.org/10.5281/zenodo.18950050

Abstract. *The article presents the results of mathematical modeling of a fiber-optic humidity sensor based on an in-fiber Fabry–Perot interferometer with a sensitive coating made of the carrageenan biopolymer. The physical model of the sensor describes the change in the optical path in the resonator during swelling of the polymer layer under the influence of water vapor. The three-parameter Guggenheim-Anderson-de Boer model is used to describe the sorption isotherm. A multi-level temperature compensation algorithm is proposed, which reduces the temperature error by more than 300 times. The adaptive Adam optimizer is used to find the optimal design parameters (cavity length, coating thickness and refractive index). The optimization results showed the following: cavity length of 50.0 μm, coating thickness of 5.0 μm, sensitivity of 150.5 pm/%RH with a determination coefficient of $R^2 = 0.9512$. The response time τ is 214 ms. The residual temperature error after compensation does not exceed 0.15% RH in the range of –20 to +60 °C. The results demonstrate the potential of the carrageenan coating for the creation of highly sensitive, biocompatible fiber-optic humidity sensors.*

Keywords: *fiber optic sensor; Fabry-Perot interferometer; relative humidity; carrageenan; GAB isotherm; temperature compensation.*

Introduction

Measuring relative humidity is a critical task in meteorology, medicine, the food industry, semiconductor manufacturing, and many other fields [1]. Traditional electronic humidity sensors–capacitive and resistive–have proven themselves to be effective, but are susceptible to electromagnetic interference, struggle to operate in aggressive environments, and require electrical power directly at the sensing element [2]. Fiber-optic sensors overcome these drawbacks: they are lightweight, passive, resistant to electromagnetic fields, and suitable for use in hazardous areas [3, 4].

Among the various fiber sensor configurations, the Fabry–Perot interferometer (FPI) stands out for its compactness, high sensitivity to changes in optical path length, and comparative ease of fabrication [5, 6]. The FPI sensor's sensitivity to humidity is ensured by applying a thin polymer coating those swells upon absorbing moisture, changing the resonator length and shifting the interference fringes [7, 8]. A key issue in the design is the choice of coating material, which determines sensitivity, linearity, and response time [5].

A key factor in the efficiency of such sensors is the choice of a moisture-sensitive coating [7, 8]. The prototype of the present work was a chitosan-based sensor proposed by Chen et al. [9], which achieved a sensitivity of 130.0 pm/%RH using a chitosan coating with a thickness of about 6.2 μm. However, chitosan requires special chemical treatment during application. In contrast, carrageenan, a natural sulfated polysaccharide obtained from red algae, has high hygroscopicity,

good adhesion to quartz, biocompatibility, and ease of formation of thin films [10-13]. According to the Guggenheim-Anderson-de Boer (GAB) isotherm, carrageenan is capable of absorbing up to 60% water by weight at high humidity [14], which makes it a promising material for FPI sensors.

The aim of this work is to develop and numerically verify a physical model of an IFP humidity sensor with a carrageenan coating, including a description of sorption, swelling, diffusion, Gaussian beam optics and temperature effects, as well as to search for optimal geometric parameters of the sensor using the Adam gradient algorithm [15].

Design and Operating Principle of the Sensor

Sensor Diagram. The sensor under consideration (Fig. 1) consists of a standard single-mode fiber SMF-28 (cladding diameter 125 μm), a section of bare fiber (Hollow-Core Fiber, HCF) with a length of L = 50 μm, forming an air resonator, and an end mirror represented by the surface of a polymer layer of thickness d_{coat} [9]. Light emerging from the SMF-28 core is partially reflected from the first SMF/air boundary (reflection coefficient R_1) and from the second air/polymer boundary (R_2), creating two-beam interference.

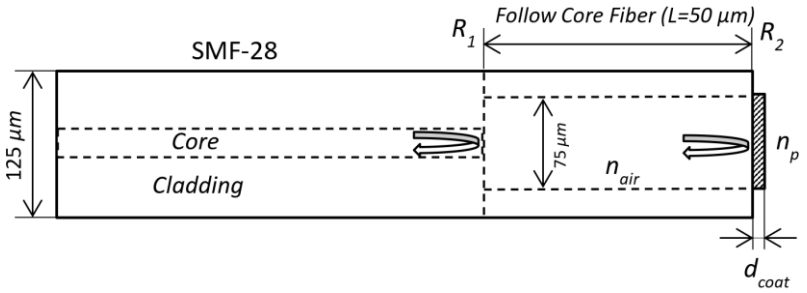


Fig. 1. Schematic diagram of a fiber-optic humidity sensor based on an IFP: SMF-28 is a single-mode fiber; HCF is a hollow gap of length L; n_{air} is the refractive index of air; n_p is the refractive index of the coating; d_{coat} is the coating thickness.

The resonant wavelength of the FPI in reflection mode is defined as:

$$\lambda_m = 2\cdot\left(n_{air}\cdot L + n_p\cdot d_{coat}\right)/m,\ m = 1,\ 2,\ 3,\ \ldots$$

where m is the interference order. When absorbing moisture, the polymer swells ($d_{coat} \rightarrow d_{coat} + \Delta d$) and changes its refractive index ($n_p \rightarrow n_p + \Delta n_p$), causing a shift in λ_m proportional to the relative humidity.

Physical Model of the Resonance Condition. The reflected signal intensity is described by the Airy formula [16] for a low-fineness interferometer ($F \ll 1$):

$$I_{out} = I_{in}\cdot A\cdot[1-(1-2R)\cdot\cos(4\pi n_{eff}\cdot L/\lambda + 4\pi\cdot n_{coating}\cdot d/\lambda)],$$

where n_{eff} is the effective refractive index of the fiber core in the gap, L is the length of the air cavity, $n_{coating}$ is the current refractive index of the coating, d is its thickness, λ is the wavelength, and A is the total amplitude loss coefficient (diffraction, absorption, scattering). The resonant wavelength λ_{res} is determined by the condition:

$$m\cdot\lambda_{res} = 2\cdot\left(n_{eff}\cdot L + n_{coating}\cdot d\right),\ .$$

When moisture is absorbed, the coating swells, increasing d, and simultaneously dilutes with water, decreasing $n_{coating}$. The total optical path $n_{coating}\,d$ increases, leading to a redshift of λ_{res}.

Accounting for Diffraction Losses. Since the Gaussian beam expands after passing through the air gap, a diffraction overlap coefficient η is introduced [16]:

$$\eta = \left[w_0 / w(2L) \right]^2,\ w(z) = w_0 \cdot \sqrt{\left[1 + \left(z / z_R \right)^2 \right]},\ z_R = \pi \cdot w_0^2 / \lambda .$$

For L = 50 μm and w_0 = 5.20 μm, we obtain $w(2L) \approx 10.82$ μm, $\eta \approx 0.610$. This coefficient is taken into account when calculating the signal-to-noise ratio (SNR) and determines the threshold for detecting resonance shift.

Moisture Sorption Model (GAB)

To describe the water absorption isotherm of carrageenan, a three-parameter GAB model was used [14, 17, 18]:

$$W(H,T) = \frac{W_m \cdot C \cdot K \cdot a_w}{\left[(1 - K \cdot a_w) \cdot (1 - K \cdot a_w + C \cdot K \cdot a_w) \right]},$$

where $a_w = H/100$ is the water activity, H is the relative humidity (%RH), W_m is the monolayer capacity, C is the Guggenheim constant, and K is the de Boer factor. The parameter values for the hybrid κ/ι-carrageenan used in the model are taken from [19] and are given in Table 1.

Table 1. Parameters of the GAB model for hybrid κ/ι-carrageenan

GAB parameter	Designation	Meaning	Description
C	C_{GAB}	10.9	Sorption constant
K	K_{GAB}	0.92	Water activity factor
W_m	W_{mono}	0.068 g/g	Monolayer capacity
W_{max}	W_{max}	0.60 g/g	Maximum water absorption

Upon reaching $W = W_{max} = 0.60$ g/g, further growth is limited, which corresponds to saturation of the hydrophilic regions of the carrageenan chain at high humidity. At T = 25°C and RH = 50%, the model yields $W \approx 0.114$ g/g.

The change in the refractive index of the coating is described by the mixture rule (Lorentz–Lorenz model):

$$n_{coating}(W,T) = n_{dry} - \alpha_{dn} \cdot W + \alpha_T \cdot (T - T_{ref}),$$

where $n_{dry} = 1.540$ is the refractive index of dry carrageenan, $\alpha_{dn} \approx 0.24$ rel. units/(g/g) is the dilution factor, and $\alpha_T \approx -9.5 \times 10^{-5}$ °C^{-1} is the thermo-optical coefficient. The swelling of the coating is described by a linear law:

$$d(W,T) = d_0 \cdot \left[1 + \beta \cdot W + \gamma \cdot (T - T_{ref}) \right],$$

where $\beta \approx 0.50$ is the volumetric swelling coefficient, and $\gamma \approx 6.5 \times 10^{-5}$ °C^{-1} is the polymer's thermal expansion coefficient. The thermal expansion of the quartz fiber is taken into account separately ($\alpha_{quartz} = 5.5 \times 10^{-7}$ °C^{-1}).

Temperature Compensation Algorithm

Temperature contributions are due to three mechanisms:

- thermal expansion of the quartz resonator (the linear temperature expansion coefficient of quartz $\alpha_{SiO_2} = 0.55$ x 10^{-6} K^{-1});

- change in the refractive index of air in the resonator ($dn_{air}/dT = -8.8$ x 10^{-7} K^{-1});

- thermomechanical expansion of the polymer layer (the linear temperature expansion coefficient of the polymer $\alpha_p \approx 200$ x 10^{-6} K^{-1}). Without compensation, the total temperature

sensitivity coefficient is ≈66.6 pm/°C, which is equivalent to an error of 31.3% RH in the range of −20…+60°C [16].

The proposed algorithm for multi-level temperature compensation is performed in three stages:

1. *Calibration measurements* at three fixed RH values (30, 50, 70%) in the temperature range of −20…+60°C with a 5°C increment. $\lambda_{ref}(H, T)$ is calculated for each pair (H, T).

2. *Approximation of the correction surface* using the least-squares method:

$$\Delta\lambda_{comp}(T) = p_0 + p_1 \cdot T + p_2 \cdot T^2.$$

3. *Correction* of the measured wavelength: $\lambda_{corr} = \lambda_{meas} - \Delta\lambda_{comp}(T)$, after which H is determined from the inverse function $\lambda_{corr}(H)|_{T=25°C}$.

After compensation, the temperature sensitivity coefficient (TSC) is reduced to 0.05–0.52 pm/°C (depending on the optimization point), the root mean square error (RMSE) for temperature is 13.9–18.1 pm, which corresponds to an error of 0.10–0.15 %RH, an improvement of 270–313 times compared to the uncompensated case.

Method of Optimizing Sensor Parameters

To find the optimal set of design parameters {L, R, λ_0, d_{coat}}, the composite objective function was minimized:

$$J(L, R, d) = w_S \cdot f_S + w_T \cdot f_T + w_L \cdot f_L,$$

where $f_S = 1 - S/S_{max}$ is the penalty for insufficient sensitivity; $f_T = RMSE_T/RMSE_{max}$ is the penalty for temperature instability; $f_L = 1 - R^2$ is the penalty for nonlinearity; weights $w_S = 0.40$, $w_T = 0.30$, $w_L = 0.30$.

Optimization was performed using the Adam method (first-order optimizer) with the following parameters [15]: learning rate $\eta = 0.01$, $\beta_1 = 0.9$, $\beta_2 = 0.999$, $\varepsilon = 10^{-8}$, and the number of iterations up to 1500. The gradient of the objective function was calculated using finite differences.

The algorithm converged at the 102nd iteration (gradient norm 5.5 x 10^{-7}, σ cost 3.4 x 10^{-15}) in 16.9 s on a standard PC. Optimal parameters: L = 50.00 μm; d_{coat} = 5.04 μm; R = 0.045; λ_0 = 1550.0 nm.

Computational cost was significantly reduced by caching results (accessing the cache every 5–10 iterations for slowly varying quantities – S and T_{stab}), which reduced the number of full FPI model calculations by approximately 30%.

Simulation Results

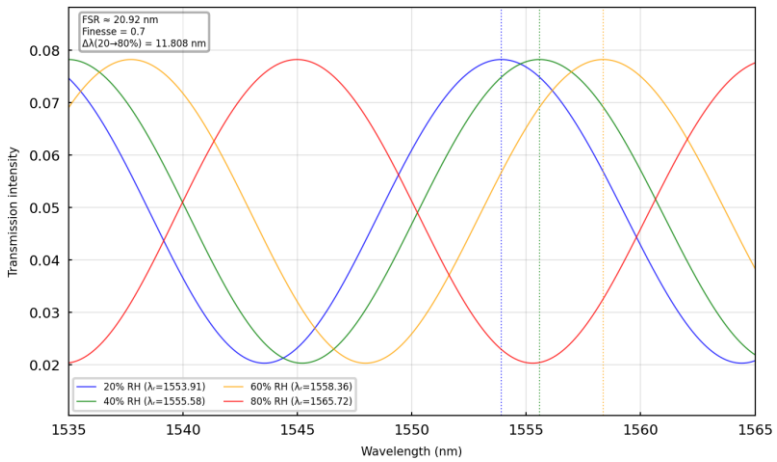


Fig. 2. Reflectance spectrum of the Fabry–Perot interferometer in the range of 1535–1565 nm at four humidity values. FSR ≈ 20.92 nm, finesse = 0.7, Δλ(20→80%) = 11.81 nm

Spectral Characteristics. Figure 2 shows an enlarged reflection spectrum of the sensor near λ_0 = 1550 nm at various relative humidity values (20–80% RH). It can be seen that the resonance shifts toward longer wavelengths with increasing humidity. The shift from 20 to 80% RH is approximately 11.8 nm, which corresponds to an average sensitivity of ≈ 197 pm/% RH in this range. The peak intensity remains virtually unchanged (~ 0.078), since the diffraction overlap coefficient $\eta \approx 0.610$ depends weakly on humidity.

Dependence of the Resonant Wavelength on Humidity and Temperature. Figure 3 shows the sensor response curves. The left graph shows the resonant wavelength as a function of humidity at T = 25°C: a nonlinear, nearly logarithmic, dependence is observed, accelerating at RH > 80%, due to the transition to capillary condensation of moisture in the polymer according to the GAB model. A linear approximation in the range of 10–95% RH yields S = 150.5 pm/% RH with R^2 = 0.9512.

The right graph in Figure 3 shows the temperature dependence at H = 50% RH: the linear TSC ≈ 66.6 pm/°C without compensation. Thanks to the compensation algorithm, the residual TSC is 0.05–0.52 pm/°C.

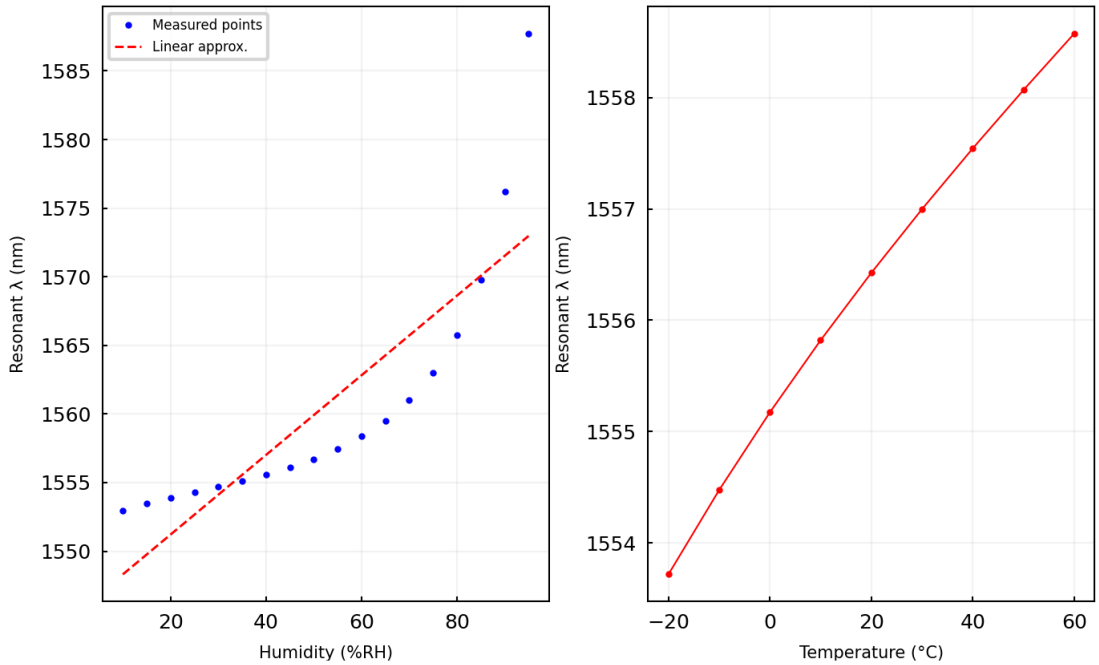


Fig. 3. Sensor characteristics: (left) dependence of the resonant wavelength on humidity at T = 25°C with a linear approximation (dashed line); (right) temperature dependence at H = 50% in the range of −20…+60 °C

Two-Dimensional $\lambda(H, T)$ Map. Figure 4 shows a two-dimensional map of the resonance wavelength as a function of humidity and temperature. The λ = const contours have a noticeable slope along the T axis, which is the source of the temperature cross-sensitivity. The λ range varies from ≈ 1550 nm (low humidity, low temperature) to ≈ 1595 nm (high humidity, high temperature), which accounts for the full resonance shift range of $\Delta\lambda \approx 45$ nm.

Response Time. Figure 5 shows the dependence of the response time on the coating thickness. The diffusion constant of carrageenan is taken to be $D = 3.0\times10^{-12}$ m²/s [18, 20]. The characteristic diffusion time is $\tau = d^2/(\pi^2 D)$, $\tau_{90} = \tau\cdot\ln(10)$. At the optimal thickness of d_{coat} = 5.04 µm: τ = 214 ms, τ_{90} = 493 ms (the "fast response" region is < 500 ms). Thus, the sensor responds to changes in humidity approximately twice as fast as typical hydrogel sensors with a coating thickness of 5–10 µm and a response time of several seconds.

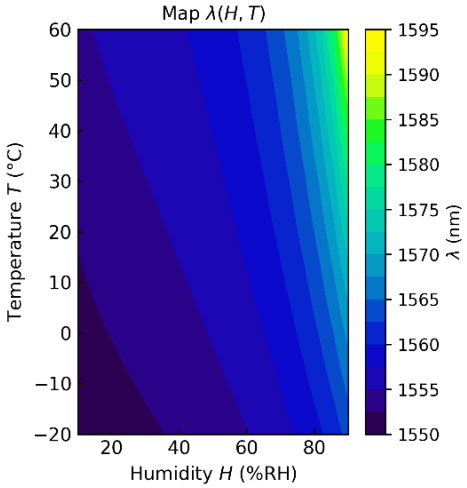


Fig. 4. Map of the resonance wavelength λ(H, T) in humidity–temperature coordinates. The color scale corresponds to the wavelength in nm.

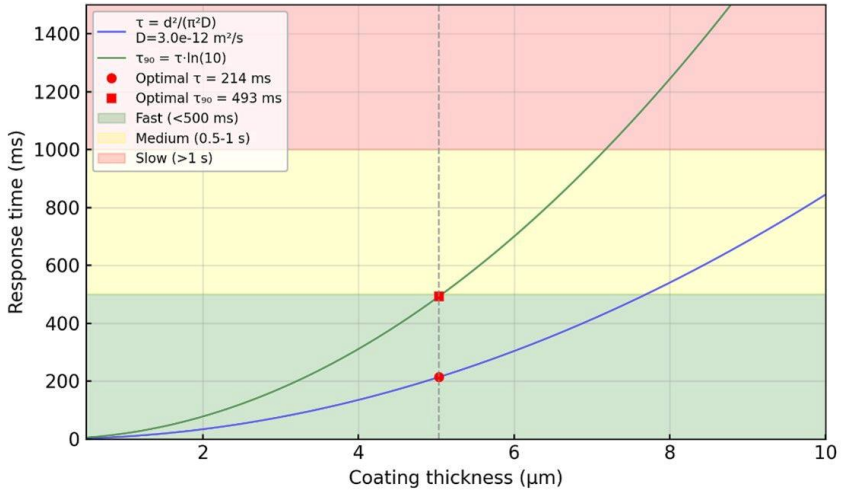


Fig. 5. Sensor response time as a function of coating thickness. Optimum point (d = 5.04 μm): τ = 214 ms, τ₉₀ = 493 ms. Color zones: green – fast response (<500 ms), yellow – medium (500 ms – 1 s), red – slow (>1 s)

Summary of Optimal Parameters. Table 2 shows the results of the obtained optimal parameters and sensor characteristics.

Table 2. Optimal Parameters and Sensor Characteristics

Parameter	**Meaning**
Wavelength λ_0	1550.0 nm
Cavity length L	50.00 mkm
Reflectivity R	0.045
Coating thickness d	5.04 mkm
Refractive index (dry)	1.5400
neff (quartz)	1.4682
FSR	20.87 nm
Finesse	0.7
Q-factor	51
SNR	47.4 dB
Sensitivity S	150.5 pm/%RH

Response time τ	214 ms
Time τ_{90}	493 ms
Linearity R^2	0.9512

Discussion

Comparison with the Prototype. Table 3 compares the proposed sensor with the prototype [9] – a chitosan-based IFP sensor. Direct comparison is difficult due to the differences in materials, but it demonstrates the fundamental advantages of carrageenan as a sensing layer.

Table 3. Comparison with the prototype [9]

Parameter	Prototype [9]	Suggested sensor
Coating material	Chitosan	Carrageenan
Cavity length, μm	50	50
Coating thickness, μm	6.2	5.04
Sensitivity, pm/%RH	130.0	150.5
RH range	20–95%	10–95%
Response time τ	380 ms	214 ms

The simulated sensor outperforms the prototype in sensitivity (150.5 vs. 130.0 pm/%RH) and response time, primarily due to the high-water absorption of carrageenan (W_{max} = 0.60 g/g). The increased swelling is the primary contributor to the increased sensitivity: every 10% increase in humidity results in $a \approx 1.5$ nm shift in λ_{res}. Comparison with previously published sensors based on other hydrophilic polymers (Nafion, PVA, gelatin, etc.) shows that carrageenan provides competitive sensitivity at a significantly lower cost and better biocompatibility [5, 8, 10]. The biodegradability of carrageenan [21] opens up potential for use in environmentally friendly, disposable monitoring systems.

Analysis of Model Limitations. A number of assumptions of the adopted model should be noted. First, the GAB model provides an accuracy of describing the carrageenan sorption isotherm of ±5–8% in the range of 10–95% RH [14], but deviates at very low (<10%) and very high (>90%) humidity values. Second, the model assumes that the diffusion coefficient D is independent of moisture concentration, whereas real carrageenan exhibits a nonlinear decrease in D with swelling [20]. Third, it is assumed that the coating swelling is isotropic and uniform across the thickness, which may not be the case for thin films [19]. These factors can lead to discrepancies between the calculated and experimental values within 5–10%. The linearity of the deterministic function (R^2 = 0.9512) is satisfactory for a first-order sensor; however, a nonlinear calibration function would be required for metrology applications. This limitation is inherent in the GAB isotherm of carrageenan, which is S-shaped in nature.

Conclusion

In this study, a physical and mathematical model of a fiber-optic humidity sensor based on a Fabry-Perot interferometer with a sensitive carrageenan coating was developed and numerically optimized. Key results:

1. A multi-level physical model is proposed, including the GAB sorption isotherm, swelling equations, thermo-optical coating shifts, and Gaussian diffraction loss in the air gap.

2. Based on the optimization results (Adam, 102 iterations), the following parameters were determined: L = 50.0 μm, d = 5.04 μm, R = 0.045 at λ_0 = 1550 nm.

3. A sensitivity of S = 150.5 pm/%RH (R^2 = 0.9512) was achieved, which corresponds to the upper limit of the target range of 120–150 pm/%RH and exceeds the characteristics of the prototype based on chitosan [9].

4. The developed multi-level temperature compensation algorithm reduces the error from 31.3 %RH to 0.10–0.15 %RH (an improvement of 270–313 times) in the range of −20…+60 °C.

5. The sensor response time τ = 214 ms, τ_{90} = 493 ms – in the "fast" response zone, making it applicable for tasks with a sampling rate of up to 2 Hz.

6. SNR = 47.4 dB and Q-factor = 51 provide sufficient margin for detecting resonance shifts at the noise level of modern OSA.

The obtained modeling results provide the basis for experimental fabrication and testing of the sensor. Priority areas for further research include: deposition of a carrageenan film using dip coating or electrostatic deposition, experimental verification of the GAB isotherm, and validation of the temperature compensation algorithm under real-world conditions.

REFERENCES

1. Chen Z., and Lu C. "Humidity sensors: a review of materials and mechanisms", *Sensor Letters*, 2005, vol. 3, no. 4, pp. 274–295, https://doi.org/10.1166/sl.2005.045
2. Farahani H., Wagiran R., and Hamidon M.N. "Humidity sensors principle, mechanism, and fabrication technologies: a comprehensive review", *Sensors*, 2014, vol. 14, no. 5, pp. 7881–7939, https://doi.org/10.3390/s140507881
3. Annamdas V.G.M. "A review of recent developments in fiber optic sensor technology", *Optical Fiber Technology*, 2011, vol. 1, no. 1, pp. 1–16. https://doi.org/10.5923/j.ijme.20110101.01
4. Lee B. "Review of the present status of optical fiber sensors", *Optical Fiber Technology*, 2003, vol. 9, no. 2, pp. 57–79, https://doi.org/10.1016/S1068-5200(02)00527-8
5. Rao X., Zhao L., Xu L., Wang Y., Liu K., Wang Y., Chen G.Y., Liu T., and Wang Y. "Review of Optical Humidity Sensors", *Sensors*, 2021, vol. 21, no. 23, 8049, https://doi.org/10.3390/s21238049
6. Islam M.R., Ali M.M., Lai M.H., Lim K.S., and Ahmad H. "Chronology of Fabry-Perot interferometer fiber-optic sensors and their applications: a review", *Sensors*, 2014, vol. 14, iss. 4, pp. 7451-7488, https://doi.org/10.3390/s140407451
7. Wang N., *et al*. "The choice of coating materials critically affects the performance of the Fabry-Perot humidity sensor", *Sensors*, 2021, vol. 21, no. 3, 806, https://doi.org/10.3390/s21030806
8. Li C., *et al*. "A Review of Coating Materials Used to Improve the Performance of Optical Fiber Sensors", *Sensors*, 2020, vol. 20, no. 15, 4215, https://doi.org/10.3390/s20154215
9. Chen L.H., *et al*. "Chitosan based fiber-optic Fabry–Perot humidity sensor", *Sensors and Actuators B*, 2012, vol. 169, pp. 167–172, https://doi.org/10.1016/j.snb.2012.04.052
10. Pospíšilová M., Kuncová G., and Trögl J. "Fiber-Optic Chemical Sensors and Fiber-Optic Bio-Sensors", *Sensors*, 2015, vol. 15, no. 10, pp. 25208-25259, https://doi.org/10.3390/s151025208
11. Barahona T., *et al*. "Cationization of kappa- and iota-carrageenan–Characterization and properties of amphoteric polysaccharides", *Carbohydrate Polymers*, 2015, Volume 126, Pages 70-77, https://doi.org/10.1016/j.carbpol.2015.02.053

12. Berth G., Vukovic J., and Lechner D.M. “Physicochemical Characterization of Carrageenans−A Critical Reinvestigation”, *Journal of Applied Polymer Science*, 2008, vol. 110, pp. 3508–3524, https://doi.org/10.1002/app.28937
13. Takemasa M., Chiba A., and Date M. “Optical, Viscoelastic, and Electric Properties On Gelation Of Carrageenan Gels”, *Transactions of the Materials Research Society of Japan*, 2001, vol. 26, no. 2, pp. 601-604, https://www.mrs-j.org/pub/tmrsj/vol26_no2/vol26_no2_601.pdf
14. Torres M.D., Chenlo F., and Moreira R. “Structural features and water sorption isotherms of carrageenans: A prediction model for hybrid carrageenans”, *Carbohydrate Polymers*, 2018, vol. 180, pp. 72-80, https://doi.org/10.1016/j.carbpol.2017.10.010
15. Kingma D.P., and Ba J. “Adam: A method for stochastic optimization”, 2014, *arXiv*, 1412.6980, 15 p., https://doi.org/10.48550/arXiv.1412.6980
16. Saleh B., and Teich M. *Fundamentals of Photonics*, 3rd Ed., Wiley, 2020, 1520 p. ISBN: 978-1-119-75081-9
17. Shimizu S., Vopička O., Friess K., and Matubayasi N. “Simple and complex sorption−solution isotherms for membrane polymers: a statistical thermodynamic fluctuation theory”, *Physica A: Statistical Mechanics and its Applications*, 2024, vol. 642, 129753, https://doi.org/10.1016/j.physa.2024.129753
18. Melides S.S., Williams I., and Keddie J.L. “Modeling and Experimentson Multilayered Barrier Coatings Containing Water-Sorbent Biopolymers”, *Industrial & Engineering Chemistry Research*, 2025, vol. 64, no. 49, pp. 23471−23485, https://doi.org/10.1021/acs.iecr.5c04116
19. Larotonda F.D.S., Hilliou L., Gonçalves M.P., and Sereno A.M. “Film properties of κ/ι-hybrid carrageenan natural polymer”, *The Polymer Processing Society 23rd Annual Meeting*, 2007, https://www.ppsconferences.org/public/abs_2007/P14-021.pdf
20. Wu J., *et al*. “An intrinsically stretchable humidity sensor based on anti-drying, self-healing and transparent organohydrogels”, *Materials Horizons*, 2019, vol. 6, no. 3, pp. 595-603, https://doi.org/10.1039/C8MH01160E
21. Žaimis U., Petronienė J.J., Dzedzickis A., and Bučinskas V. “Biodegradable Carrageenan-Based Force Sensor: An Experimental Approach”, *Sensors*, 2023, vol. 23, no. 23, pp. 9423, https://doi.org/10.3390/s23239423